Optics & Laser Technology 197 (2026) 114847

Contents lists available at ScienceDirect

Optics and Laser Technology

journal homepage: www.elsevier.com/locate/optlastec

Full length article

Comparison of QEPAS and BF-QEPAS approaches for methane and ethane sequential detection in the near-IR spectral range

Luigi Melchiorre [a,b], Giansergio Menduni [a,*], Giovanni Magno [b], Liam O'Faolain [c,d], Pietro Patimisco [a,e], Vincenzo Spagnolo [a,e], Angelo Sampaolo [a,e]

[a] PolySenSe Laboratory, Interuniversity Physics Department, Polytechnic University and University of Bari 70126 Bari, Italy
[b] NanoPhotonics and Electromagnetics Group, Electrical and Information Engineering Department, Polytechnic University of Bari 70125 Bari, Italy
[c] Centre for Advanced Photonics and Process Analysis, Munster Technological University, T12 P928 Cork, Ireland
[d] Tyndall National Institute, T12 PX46 Cork, Ireland
[e] PolySenSe Innovations S.r.l., Via G. Amendola 173, 70125 Bari, Italy

ARTICLE INFO

Keywords:
Beat-frequency
Environmental monitoring
Ethane
Methane
Quartz tuning fork
Quartz-enhanced photoacoustic spectroscopy

ABSTRACT

This paper presents a comparison between quartz-enhanced photoacoustic spectroscopy (QEPAS) and beat-frequency QEPAS (BF-QEPAS) techniques for the sequential detection of methane (C1) and ethane (C2) in the near-infrared spectral range. Both approaches exploit a T-shaped quartz tuning fork (QTF)—coupled with acoustic resonator tubes—as sensitive element but differ fundamentally in the signal generation and acquisition methods. While conventional QEPAS-based approach requires periodic QTF characterization and longer acquisition time, BF-QEPAS enables simultaneous measurement of target gas concentration, QTF resonance frequency and quality factor through analysis of transient response signals. Experiments were performed using a laser diode emitting at a central wavelength of 1683.53 nm, targeting C1 and C2 absorption features. Our results demonstrate that the BF-QEPAS approach significantly reduces measurement time from minutes to few seconds and maintains comparable detection sensitivity, also for broadband absorbers such as ethane. For methane, minimum detection limits (MDLs) of 1.7 parts-per-million (ppm) and 5 ppm were achieved with QEPAS and BF-QEPAS techniques, respectively, while for ethane MDLs of 20 ppm and 62 ppm were obtained, respectively. The BF-QEPAS technique enables continuous, uninterrupted monitoring of both target gases in sequential detection mode, with the simultaneous validation of the measurement through the evaluation of the QTF resonance parameters.

1. Introduction

Trace gas detection of methane and ethane has become increasingly critical in environmental monitoring, industrial safety, and energy infrastructure maintenance [1–5]. These hydrocarbons constitute primary components of natural gas and are emitted through various industrial processes, agricultural activities, and natural sources [6–11]. According to the latest Global Methane Budget, methane emissions now total about 575 million metric tons per year (2010–2019 average), significantly higher than earlier estimates [12–14].

In many real-world scenarios, methane (C1) and ethane (C2) coexist and require sequential monitoring [15–17]. Indeed, natural gas leaks contain both components in varying ratios, providing fingerprints for source identification and characterization and leak severity assessment [18–20]. For instance, industrial process monitoring demands rapid sequential detection to track compositional changes in real-time [21], while environmental studies require distinguishing between biogenic sources (predominantly methane) and thermogenic sources (containing both gases) [22,23]. However, conventional detection methods often have limitations in field applications, requiring complex sampling procedures, bulky instrumentation, or offering inadequate sensitivity and response time [24–26]. Moreover, these methods typically necessitate separate measurement systems for each gas species, increasing complexity, cost, and measurement time [27–29].

Quartz-enhanced photoacoustic spectroscopy (QEPAS), first demonstrated by Kosterev *et al.* in 2002 [30], is a highly sensitive, selective and well-established optical technique for trace gas detection [31–33]. In QEPAS, quartz tuning forks (QTFs) are employed as sharply

* Corresponding author.
E-mail address: giansergio.menduni@poliba.it (G. Menduni).

https://doi.org/10.1016/j.optlastec.2026.114847
Received 3 September 2025; Received in revised form 9 December 2025; Accepted 27 January 2026
Available online 31 January 2026

resonant acoustic transducers to detect pressure waves generated when modulated laser light is absorbed by target gas molecules, *i.e.*, through the photoacoustic effect. The piezoelectric property of quartz allows the conversion of the sound wave into an electric signal [34–36]. Furthermore, in recent years these quartz resonators have been employed as photodetectors, exploiting piezoelectricity to transduce light-induced thermoelastic deformation [37,38]. QTFs high and flat spectral responsivity measured in the 1.65–10.34 μm wavelength range [39] makes them well suited for the implementations in various spectroscopy techniques [40,41].

Conventional QEPAS implementations face significant challenges when applied to multi-species detection [42], because they could require periodic calibration to account for possible drifts in the QTF resonance parameters [43], and sequential measurements of multiple gases could demand extended acquisition times, limiting real-time monitoring capabilities [44].

Beat-frequency QEPAS (BF-QEPAS), introduced by Wu *et al.* in 2017 [45], represents a significant advancement in addressing these limitations [46]. From the analysis of the beat signal generated by a detuned photoacoustic excitation of the QTF with respect to its resonance frequency [44], this approach allows the simultaneous measurement of the gas concentration and the QTF resonance properties, *i.e.* the resonance frequency f_r and the quality factor Q, thus eliminating the need for periodic resonator characterization [47–49].

Within the aims and scopes of our experiment, and due to their light weight, compactness and low power consumption, fiber-coupled near-infrared (near-IR) laser diodes represent the best choice in terms of optical sources for sensing in real-world scenarios. Nevertheless, the sequential detection of C1 and C2 presents peculiar challenges due to their spectral characteristics in the near-IR spectral region, as already discussed in Ref. [50]. Indeed, methane exhibits well-resolved Lorentzian-like absorption features with large cross-sections [51] that allows an accurate photoacoustic signal generation and QTF parameter retrieval with the BF-QEPAS technique [50]. In contrast, ethane is characterized by a complex band structure with multiple overlapping optical transitions [52,53], resulting in a BF-QEPAS signal whose peaks' interpolation poses unavoidable difficulties in extracting the QTF parameters. These experimental evidences set the basis for developing a single detection scheme implementing BF-QEPAS that can leverage the favorable properties of methane for the measurement of the QTF parameters while preserving an affordable level of sensitivity for the more critical detection of ethane [54].

In this context, we thus present here a comparison between QEPAS and BF-QEPAS approaches for the sequential detection of methane and ethane in the near-IR spectral range. Our experimental apparatus incorporates a laser diode emitting at a central wavelength of 1683.53 nm, capable of targeting absorption features of both gases, and an acoustic detection module (ADM) that houses a T-shaped QTF, coupled with acoustic resonator tubes, as sensitive element. We demonstrate that methane BF-QEPAS signal can be efficiently exploited for *quasi* real-time retrieval of both C1 concentration and QTF parameters, while the broadband feature of C2 allows only the measurement of ethane concentration with the BF-QEPAS technique. To the best of our knowledge, no previous study has compared QEPAS and BF-QEPAS for sequential CH_4/C_2H_6 detection and for the different suitability of each molecule to retrieve QTF parameters.

2. Experimental setup

The experimental apparatus used to compare QEPAS and BF-QEPAS techniques for C1 and C2 detection is depicted in Fig. 1.

The sensing architecture consists of three sections: the gas handling system (shown in the dashed green section in Fig. 1), the optical detection module (in the dashed violet one), and the electronic signal processing unit (in the dashed blue section). The gas handling section includes five certified gas cylinders containing 2% CH_4 in nitrogen (N_2), 0.1% CH_4 in N_2, 1% C_2H_6 in N_2, 0.1% C_2H_6 in N_2, and pure N_2 (*i.e.*, 100%) for target gas dilutions. These cylinders are connected to a gas blender (MCQ Instruments, GB6000) to provide precise gas mixtures for the sensor calibration in the 0–1% concentration range for both C1 and C2. The 50 standard cubic centimeters per minute (SCCM) gas flow is injected into a commercial ADM (Thorlabs GmbH, ADM01) [55] by

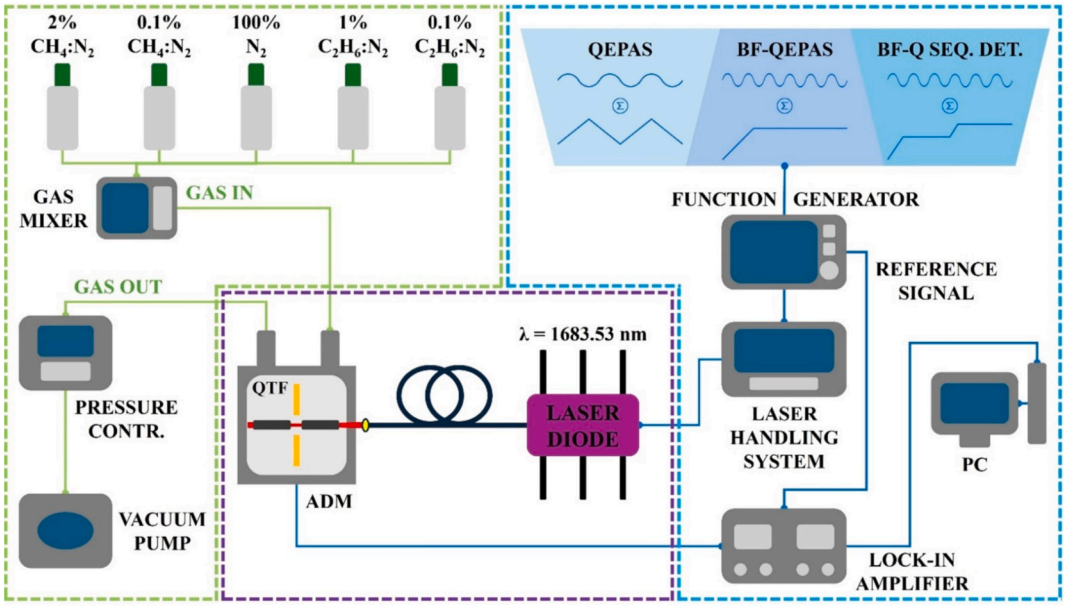

Fig. 1. Schematic of the experimental setup for QEPAS and BF-QEPAS comparison. The dashed green section shows the gas handling system with certified gas cylinders and flow/pressure control components for precise gas mixture preparation (0–1% calibration range for both C1 and C2). The dashed violet section depicts the optical detection module with the ADM including a T-shaped QTF coupled with acoustic resonator tubes. The dashed blue section illustrates the electronic signal processing unit composed of the function generator, the laser diode handling system, and the lock-in amplifier for signal demodulation and analysis. The upper right inset shows the three operating modes implemented in this study: QEPAS and BF-QEPAS for C1 and C2 sensor calibration, and BF-QEPAS with double staircase ramp for sequential detection of both target gases.

means of a vacuum pump (KNF DAC GmbH, N813.4ANE), and a pressure controller (Alicat Scientific, MC Series) allow maintaining a stable pressure condition of 750 Torr in the gas line.

The exciting laser source consists of a distributed-feedback (DFB) pigtailed laser diode (Eblana Photonics Ltd., EP1684-0-DM-B06-FA) emitting at a central wavelength of 1683.53 nm when operated at 15 °C, with a maximum optical power of ≈ 9 mW at an injected current of 120 mA. This source was selected since its tuning range covers a spectral window in which the C1 and C2 absorption features can be effectively excited through a single wavelength scan at a fixed temperature. Specifically, the laser diode can address a six-line cluster of methane located at 5938.12 cm^{-1} [51] and an ethane absorption band centered at 5937.3 cm^{-1} [52,54], both resulting from carbon (C)–hydrogen (H) stretching overtone transitions [53]. The laser diode output is coupled with a fiber collimator (OZ Optics Ltd., LPC Series) and then aligned to the ADM, which houses the custom spectrophone that has been demonstrated to provide the best performances in terms of signal-to-noise ratio (SNR) for QEPAS detection [50]. This spectrophone is composed of a T-shaped QTF acoustically coupled with two 12.4 mm-long acoustic resonator tubes (with an inner diameter of 1.6 mm) [55]. The output laser beam is precisely aligned between the QTF prongs and inside the tubes without hitting them, thus maximizing the photoacoustic signal and minimizing background noise.

The signal processing unit consists of a compact laser handling system (Thorlabs GmbH, CLD1010) that controls the laser diode through a current driver and a temperature controller to maintain a working temperature of 15 °C. An arbitrary waveform generator (Tektronix Inc., AFG31052) provides the required modulation signals for both QEPAS and BF-QEPAS measurements. The wavelength modulation in the QEPAS approach is achieved by applying a sine wave at half of the QTF resonance frequency (*i.e.*, $f_r/2$) to the laser injection current, while a slow triangle ramp allow to scan the laser wavelength across the selected C1 and C2 absorption features [56]. In contrast, BF-QEPAS employs a modulation frequency slightly detuned from the QTF resonance one (*i.e.*, $f_{MOD} = f_r \pm \Delta f$) combined with a fast staircase ramp for wavelength scanning, as shown in the inset of Fig. 1. The piezocurrent generated by the QTF is converted into a voltage signal via a transimpedance amplifier and subsequently processed by a lock-in amplifier (Zurich Ins., MLFI 500 kHz). The lock-in integration time constant was set to 100 ms (with a sampling rate of 3.27 Sa/s) and to 5.097 ms (sampling rate of 52.32 Sa/s) in the QEPAS and BF-QEPAS measurements, respectively. As typically reported in literature, the second harmonic (2*f*)-wavelength modulation spectroscopy (WMS) technique was employed for the QEPAS acquisitions [57], while the first harmonic (1*f*)-WMS modulation technique was exploited to acquire the BF-QEPAS signals [45,58].

The optical characterization of the QTF, performed in a 1% CH_4:N_2 gas matrix, returned a f_r of 12,455.26 Hz and a *Q* of 8620.

The experimental setup allows seamless switching between three operating modes as illustrated in the inset of Fig. 1: (i) QEPAS technique with 2*f*-WMS, using a sine wave having an amplitude of 80 mVpeak-to-peak (pp) and a frequency of $f_r/2$ added to a triangle wave at 2.5 mHz to scan C1 and C2 selected absorption features; (ii) BF-QEPAS with 1*f*-WMS for C1 and C2 detection, exploiting a sine wave with an amplitude of 80 mVpp and a modulation frequency of 12,453.3 Hz (with a $\Delta f \approx 2$ Hz detuning that will be shown to optimize the BF-QEPAS signal characteristics), and a staircase ramp with a period of 5 s, having one fourth of the period composed of an edge rising at a rate as fast as 0.176 V/s for the C1 detection (0.192 V/s for the C2 detection); and (iii) BF-QEPAS with a double staircase ramp for C1 and C2 sequential detection (with a period of 10 s) optimized for multi-gas analysis.

All these listed parameters will be the results of the following investigation and optimization process.

3. Results

The sensor was initially calibrated in the QEPAS and BF-QEPAS configurations, respectively, flowing through the ADM different concentrations of methane and ethane, separately, in a gas matrix of pure N_2. The QEPAS spectra at different concentrations and the calibration curves for both hydrocarbons are shown in Fig. 2. The spectra in the following will be reported as a function of the acquisition time to easily compare in the scanning time required for QEPAS and BF-QEPAS.

Fig. 2(a) shows the spectral scans retrieved for CH_4:N_2 concentrations ranging from 0.02% to 1%. As expected from the targeted methane absorption feature centered at 5938.12 cm^{-1} [51], the C1 QEPAS scans exhibit a typical 2*f*-WMS spectra, with the characteristic second-derivative absorption profile and a background-free signal, consistently with the QEPAS signal recorded for a pure N_2 gas sample (purple solid signal in Fig. 2(a)). The 2*f*-QEPAS spectra for C_2H_6:N_2 shown in Fig. 2(b) have been acquired in the same concentration range of the C1 spectra. In the laser tuning range, the ethane absorption spectrum consists of an absorption band, with a well-resolved peak at 5937.3 cm^{-1} [59] plus additional smaller absorption sidebands, clearly visible in the measured C2 QEPAS spectra in Fig. 2(b). A linear fit was applied to retrieve the C1 and C2 calibration curves, shown in Fig. 2(c) and Fig. 2(d). The fit returned a C1 sensitivity of (549.89 ± 1.56) mV/% (slope of the purple line in Fig. 2(c)), with the R^2 value exceeding 0.9999. The ethane calibration curve (Fig. 2(d)) similarly demonstrates a linear response, with an R^2 value greater than 0.999, with a C2 sensitivity of (46.85 ± 0.22) mV/%. The linear behavior is crucial for accurate concentration measurements and validates the suitability of QEPAS technique for quantitative analysis of both gases.

The noise level of the system was determined by analyzing the standard deviation of the signal with pure N_2 flowing in the ADM. Considering a 1σ-noise level of 0.09 mV and the retrieved sensitivities, the minimum detection limits (MDLs) (with an SNR of 1) were calculated to be 1.7 parts-per-million (ppm) for CH_4 and 20 ppm for C_2H_6, with an integration time of 100 ms.

With the same experimental setup shown in Fig. 1, the BF-QEPAS technique was implemented for both C1 and C2 detection and the BF spectra in the same conditions of the QEPAS measurements, *i.e.* concentration range and pressure, are shown in Fig. 3.

Unlike QEPAS signals, which only yield concentration information, BF-QEPAS signals simultaneously provide gas concentrations and QTF resonance parameters in less than 5 s of measurements. Since 200 s are required to obtain the entire harmonic signal with QEPAS scan of the same spectral window, as shown in Fig. 2(a) and 2(b), the BF approach allows a 40-fold faster response.

Fig. 3(a) shows the BF-QEPAS spectral scans retrieved for CH_4:N_2 concentrations ranging from 0.02% to 1%. As expected, when targeting a well-isolated absorption feature [46,47], the observed signals exhibit the characteristic damped oscillations at the beat frequency of $\Delta f \approx 2$ Hz. In contrast, the signals recorded for C_2H_6:N_2 concentrations ranging from 0.02% to 1% (Fig. 3(b)) significantly differ from the BF-QEPAS spectra acquired for C1. Unlike methane, the C2 signals display significant differences in terms of secondary peak intensity and temporal spacing among them with respect to a typical BF signal related to a single feature wavelength scan. This is obviously due to the multiple optical features composing C2 spectrum. Indeed, as also reported in Fig. 2(b), the overlap of the corresponding damped oscillations leads to the irregular oscillation period in the overall BF-QEPAS signal. Furthermore, the inspection of the C2 BF-QEPAS spectra at low and high concentrations (*e.g.*, red curve and dark blue curve in Fig. 3(b)) suggests that weak absorption features, such as those at 25 s and 160 s in Fig. 2(b), strongly affect the frequency of the BF signal at ethane concentration higher than 0.2%, but are negligible at lower concentration. The highest peak values in Fig. 3(b) were used to calibrate the sensor with respect to the C_2H_6 concentrations since they are not influenced by the overlaps with other features, as also expected from Fig. 2(b)–(d).

The calibration curves derived from the BF-QEPAS peak signal values are shown in Fig. 3(c) and 3(d) for C1 and C2, respectively, both exhibiting excellent linearity across the entire concentration range, with

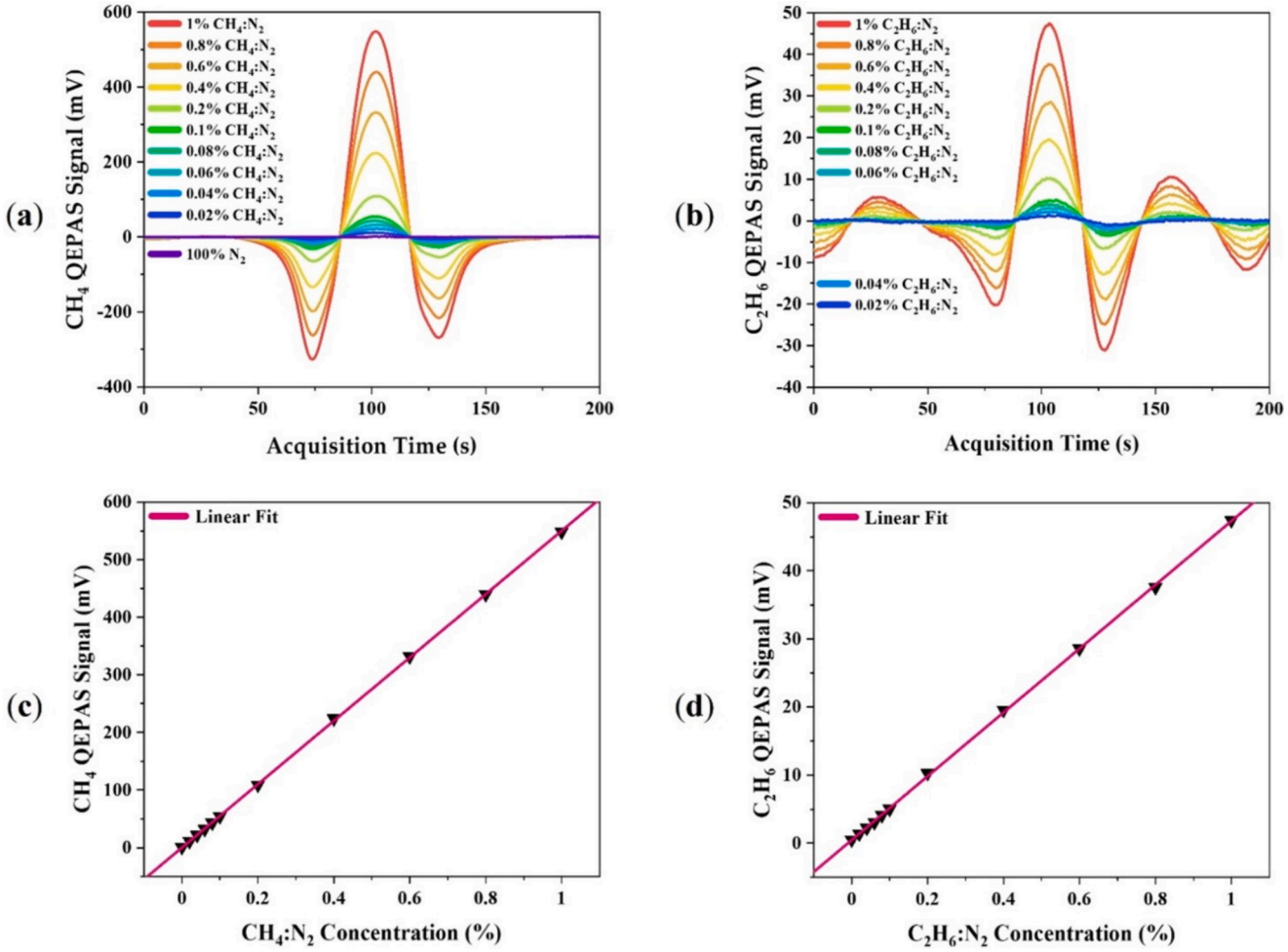

Fig. 2. (a) 2*f*-QEPAS spectra for different concentrations of CH_4 diluted in N_2; (b) 2*f*-QEPAS spectra for different concentrations of C_2H_6 diluted in N_2; (c) C1 QEPAS calibration curve; (d) C2 QEPAS calibration curve. The black triangles represent measured data while the purple solid lines represent the best linear fits of the experimental data.

R^2 values exceeding 0.999. The sensitivities derived from the linear fits are (308.38 ± 1) mV/% for CH_4 and (25.16 ± 0.12) mV/% for C_2H_6, and considering a noise level of approximately 0.16 mV—determined from the standard deviation of the BF signal with pure N_2—the calculated MDLs (SNR of 1) for the BF-QEPAS technique result 5 ppm for CH_4 and 62 ppm for C_2H_6, respectively, at an integration time of 5.097 ms. These detection limits are comparable to those achieved with conventional QEPAS, with a worsening factor of ≈ 3 for both hydrocarbons, thus indicating that BF approach allows similar MDLs but with a significant reduction in the acquisition time.

After the calibrations of C1 and C2 with both techniques, the same experimental setup was exploited to simultaneously detect methane and ethane in a nitrogen-based gas matrix, thus addressing real-world applications such as the identification of natural gas leaks in the environment [60]. Fig. 4 presents a direct comparison between QEPAS and BF-QEPAS approaches for the sequential detection of both gases, analyzing four representative gas mixtures.

The acquisition of the signals shown in Fig. 4 requires slight modifications of the ramp signal employed for the scan of the laser tuning range. While for the QEPAS spectra only the amplitude of the ramp was increased to allow the scan of both methane and ethane absorption features, two stationary levels of the same duration (5 s) in the BF-QEPAS technique were further added in the staircase ramp (see the waveforms in the inset of Fig. 1) to avoid the overlap of the C1 and C2 damped oscillations. In Fig. 4 two complete C1/C2 scans (not optimized in terms of minimum ramp affordable to gather all the information needed) are displayed. Both techniques successfully resolve CH_4 and C_2H_6 peaks, but the BF-QEPAS approach requires ≈ 10 s for the complete scan of the two selected absorption features, *i.e.*, a ≈ 50-fold reduction in the acquisition time with respect to QEPAS.

As expected from previous works [50], the QEPAS approach allows the quantification of C1 and C2 concentrations in the mixtures using the calibration curves shown in Fig. 2(c)–(d), with an average relative error as low as ≈ 2.3%.

In addition to the information on the concentration of different molecules in a mixture, the BF-QEPAS approach can provide the resonance parameters of the QTF from the analysis of the acquired signals [45]. The resonance characterization of the QTF via photoacoustic excitation and electrical excitation, pursued by exploiting the direct and indirect piezoelectric effect, respectively, will be both used as reference methods to monitor f_r and Q at different concentrations of the two analytes. The results obtained for C1, C2 concentrations varying from 0 to 1% in pure nitrogen highlight the fact that such a matrix variation does not cause an actual modification of the resonance properties, which would require a modulation frequency adjustment and a quality factor normalization [44,61]. Concerning the possibility to retrieve the same values from the BF-QEPAS spectra, focus should be placed on Fig. 4(b), where it is possible to distinguish the C1 (first 5 s of the data) and the C2 (data in the 5–10 s range) BF signals.

The calibration curves obtained (Fig. 3(c)–(d)) returned a low average relative error of ≈ 3.2% on the concentration measurement for the BF peaks labelled as C1 and C2 in Fig. 4(b). A greater discrepancy of

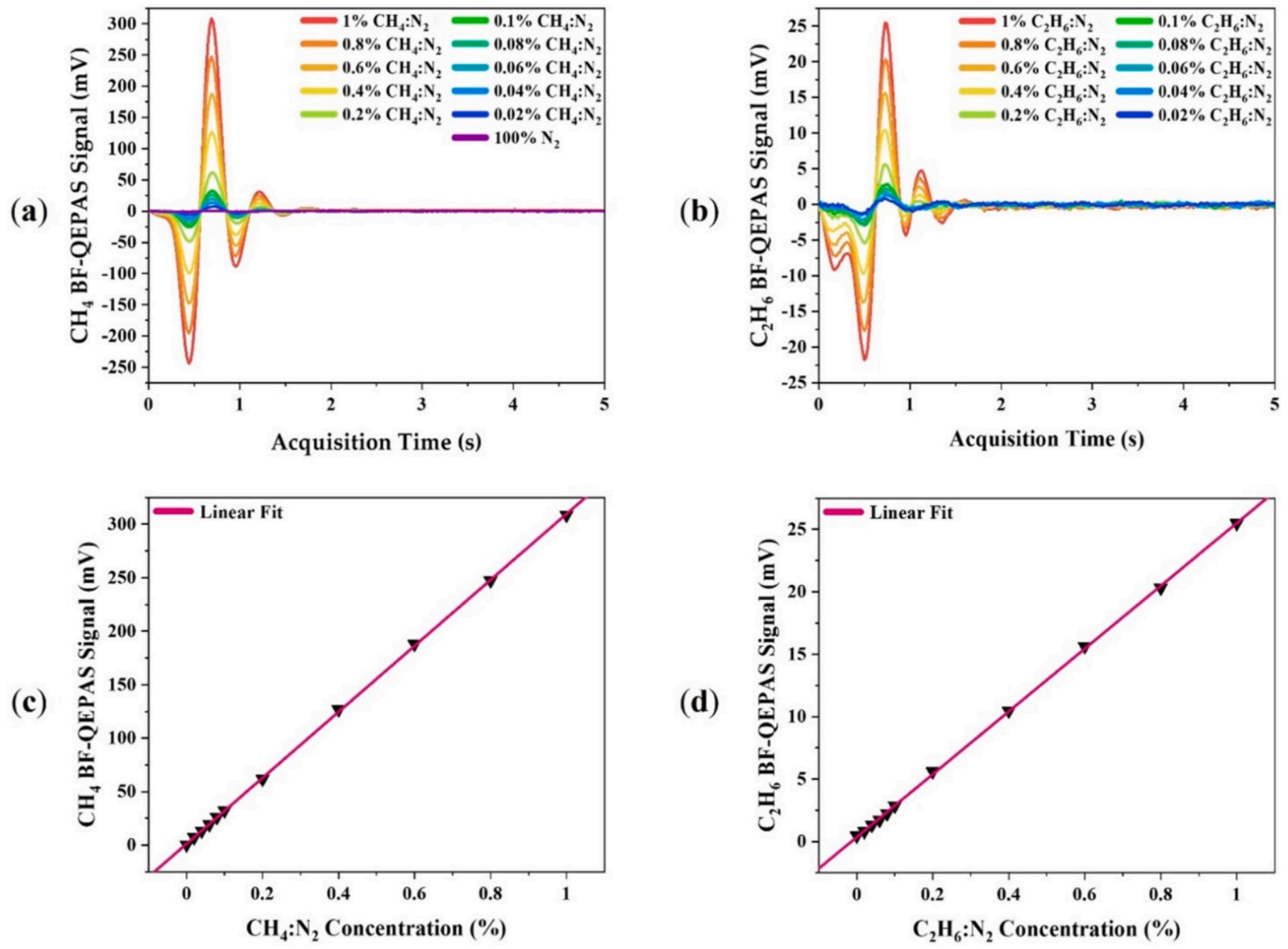

Fig. 3. (a) 1*f*-BF-QEPAS signals for different concentrations of CH_4 diluted in N_2; (b) 1*f*-BF-QEPAS signals for different concentrations of C_2H_6 diluted in N_2; (c) C1 BF-QEPAS calibration curve; (d) C2 BF-QEPAS calibration curve. The black triangles represent measured data while the purple solid line is the best linear fit of the experimental data.

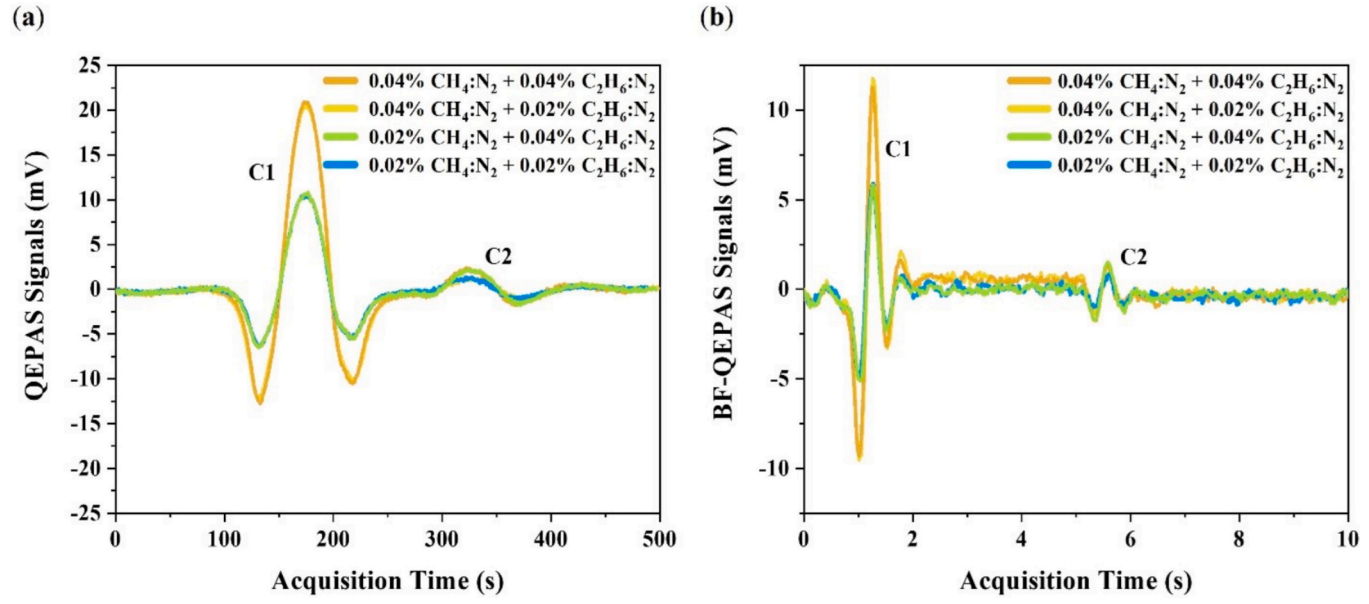

Fig. 4. Sequential detection of C1 and C2 in four representative nitrogen-based gas mixtures with (a) QEPAS and (b) BF-QEPAS technique.

≈ 5.7% was evaluated for ethane due to weaker signals that approached the detection limit. This is an indication that ethane is less appropriate for monitoring the QTF resonance properties.

To retrieve the resonance parameters, *i.e.*, QTF resonance frequency and quality factor, the following damped sine wave fitting function was applied to the BF-QEPAS signals shown in Fig. 3(a)–(b), in the time range starting from the highest peak signal value to the end of the acquired data:

$$f_{fit}(t) = A \bullet e^{-\frac{t}{\tau}} \bullet \sin\left(2 \bullet \pi \bullet \Delta f_{fit} \bullet t\right) \quad (1)$$

where A is the amplitude, τ is the exponential decay time constant and Δf_{fit} is the beat frequency of the damped sinewave. The retrieved QTF resonance frequency (f_{BF}) was determined by adding the retrieved Δf_{fit} to the laser modulation frequency (*i.e.*, f_{MOD} = 12,453.3 Hz), while the quality factor (Q_{BF}) was calculated as:

$$Q_{BF} = \pi \bullet f_{BF} \bullet \tau \quad (2)$$

In Fig. 5, the retrieved resonance frequencies ($f_{BF\text{-}C1}$) and the quality factors ($Q_{BF\text{-}C1}$) of the QTF are shown as functions of the C1 gas concentration, along with the corresponding value obtained through optical characterization of the resonator (f_r and Q). Moreover, f_r includes a ± 83.55 mHz tolerance band for the measurements derived from the normalized optical response of the QTF within 99% of its maximum amplitude. Similarly, Q is shown along with upper and lower bounds corresponding to ±1% of its value (*i.e.*, $Q_{LOW} = 0.99 \bullet Q$ and $Q_{HIGH} = 1.01 \bullet Q$), representing the maximum tolerated deviation considered for the analysis and inherited from f_r.

The results of the C1 BF-QEPAS signals analysis were obtained using a single damped sine wave fitting model, reported in Eq. (1). As shown in Fig. 5(a), the retrieved QTF resonance frequencies tend to asymptotically match f_r, at high CH_4:N_2 concentrations, while $f_{BF\text{-}C1}$ shows lower accuracy in the 0.02%–0.2% methane concentration range because of the lower SNR, although all values lie within the defined tolerance band of the measurement except for the one at 0.02% methane concentration. Similarly, the $Q_{BF\text{-}C1}$ (Fig. 5(b)) extracted value stabilizes for concentrations above 0.4% CH_4:N_2, in excellent agreement with both the optically/electrically characterized value and the measurement tolerance interval.

The stability of values (1σ-$f_{BF\text{-}C1}$ ≈ 67.4 μHz, 1σ-$Q_{BF\text{-}C1}$ ≈ 567) and the high accuracy (average relative error on f_r ≈ 4.42 ppm, average relative error on Q ≈ 4.8%) of the retrieved resonance parameters for high methane concentrations indicates that the CH_4 BF-QEPAS signal can be used to evaluate both the QTF resonance frequency and the quality factor for C1 concentrations > 1%, where the resonance properties are expected to be still unperturbed up to 10% [62], but that can actually experience sensible modifications for several tens of %. In the reported BF-QEPAS approach, f_r and Q are not estimated through predefined correction functions but are directly retrieved from each BF waveform via the damped-sine fitting model. Therefore, any variation in gas density, background composition or residual mass-loading effects is intrinsically included in the real-time evaluation of the QTF parameters. Furthermore, accurate values of f_r and Q can be extracted from high-SNR BF signals outside the 0–1% concentration range explored, since the fitting method does not impose constraints on the absolute concentration level.

Fig. 6 shows the retrieved resonance frequencies ($f_{BF\text{-}C2}$) and quality factors ($Q_{BF\text{-}C2}$) of the QTF as functions of the C_2H_6:N_2 concentrations, along with the reference value calculated from the optical characterization (f_r and Q) and the same tolerance band introduced in the C1 analysis.

The targeted absorption band of C2 makes complicated the BF-QEPAS analysis for the evaluation of QTF resonance parameters. Indeed, the fitting function in Eq. (1) applied to the high SNR 1% C_2H_6:N_2 signal (red curve in Fig. 3(a)) returned an R^2 of 0.94, confirming that the single damped sinewave model is not representative of the generated C2 BF signal at high SNRs. As shown in Fig. 2(b), the highest C2 peak detected in the laser tuning range is followed by a weaker and comparable peak (namely P2), thus suggesting that the BF signal can be considered as the linear overlap of two damped sine waves (*2-damp-sin*). Considering the ethane concentration range 0.4%–1%, the *2-damp-sin* fit returned an average $R^2 > 0.99$ for the four analyzed curves. Since the two beat frequencies extracted from the fitting sine waves strongly differ ($\Delta f_{fit\text{-}1} > 2 \bullet \Delta f_{fit\text{-}2}$), the QTF resonance parameters with the BF-QEPAS technique were extracted using the frequency of the sine wave closer to 2 Hz, experimentally employed, and the corresponding exponential decay time (blue squares in Fig. 6(a)–(b)). In contrast to the high concentration signals, the *2-damp-sin* fit does not converge for the signals relative to ethane concentrations in the 0.02%–0.2% range because the P2 values become comparable to the noise level and thus the BF signal has a single damped sine wave (*1-damp-sin*)-like shape. For this reason, the fitting function in Eq. (1) was employed to retrieve the resonance frequency and the quality factor of the QTF at low C2 concentrations (green squares in Fig. 6(a)–(b)).

The inspection of both panels in Fig. 6 highlights that the extracted parameters (green and blue squares) are not reliable for the evaluation

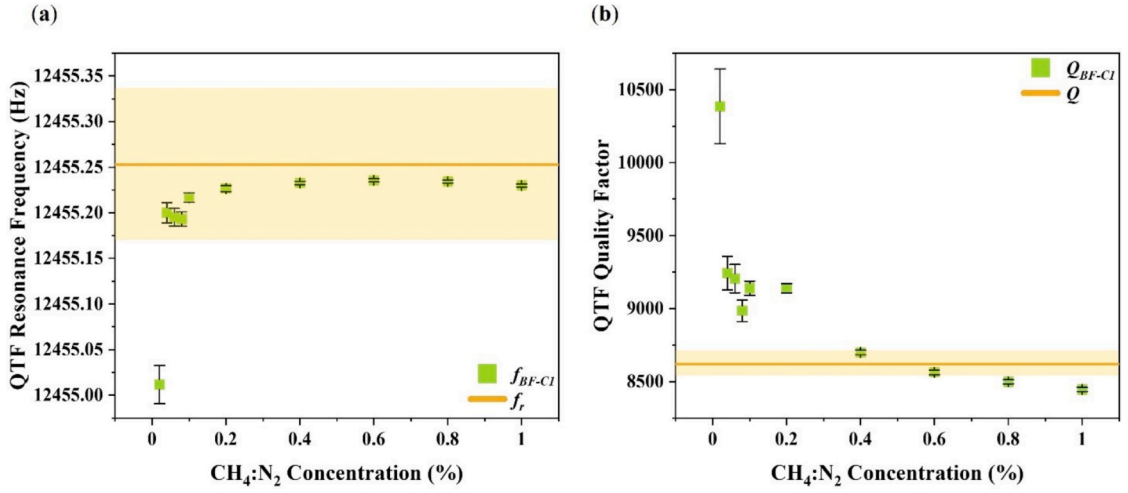

Fig. 5. QTF (a) resonance frequencies and (b) quality factors retrieved from C1 BF-QEPAS signals analysis, as a function of methane concentration. Green squares represent values retrieved through damped sine wave fitting of experimental data, while orange lines indicate reference value calculated from QTF optical characterization with the shaded yellow regions indicating the corresponding measurement tolerance band.

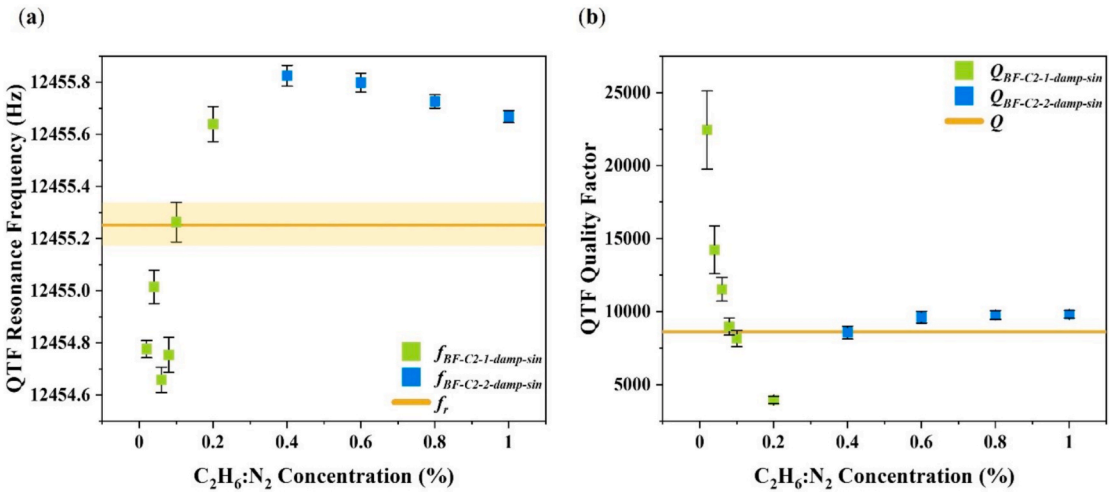

Fig. 6. QTF (a) resonance frequencies and (b) quality factors retrieved from C2 BF-QEPAS signals analysis, as a function of ethane concentration. Green and blue squares represent values retrieved through the fitting of experimental data, while orange lines indicate the reference value calculated from QTF optical characterization with the shaded yellow regions indicating the corresponding measurement tolerance band.

of the QTF resonance properties. Indeed, the high variability of the fitted data in the f_{BF} graph (> 1 Hz in Fig. 6(a)) and in the Q_{BF} graph (> 15,000 in Fig. 6(b)) confirms that the C2 BF-QEPAS signal is not suitable to provide the QTF resonance frequency and the quality factor due to the lower SNRs of the signals and the complex absorption structure of ethane in the selected tuning range.

Therefore, the comparison between the results in Figs. 5 and Fig. 6 suggests that only the analysis of C1 BF-QEPAS signal can effectively provide both f_r and Q. Since in most applications both hydrocarbons will be present in the mixture [10,17], the methane signal could be analyzed for the assessment of both the resonance frequency and the quality factor, validating the measurement, while the BF signals of C1 and C2 should provide the corresponding gas concentrations. However, the application of multiple sine-damped fit models within BF-QEPAS signal analysis could allow effective treatment of multi-peak analytes such as the case of ethane.

4. Conclusions

In summary, this work compared conventional QEPAS and BF-QEPAS for methane and ethane detection in the near-IR spectral range, addressing the critical need for rapid and multi-species gas sensing in real-world applications. While both techniques demonstrated reliable detection over a broad concentration range, BF-QEPAS provided a decisive advantage in acquisition speed, enabling sequential detection up to 50 times faster than QEPAS, with only a moderate trade-off in detection limits.

Our results further confirm that BF-QEPAS can effectively detect gases with distinct absorption characteristics. When applied to sharp spectral features, the reported technique allows the simultaneous measurement of methane concentration and QTF f_r and Q from C1 signals. Since ethane is characterized by a broadband absorption profile, we demonstrated that BF-QEPAS enabled C2 concentration measurements, though with reduced reliability in retrieving QTF resonance properties. Although this approach is inherently suitable for point-sensing technique, this architecture directly addresses the requirements of industrial leak quantification and safety monitoring, where compact, alignment-free and fast sensors are preferred over wide-area optical systems.

Future developments will aim to refine signal processing algorithms to improve parameter retrieval from complex molecular fingerprints, implement adaptive modulation strategies to tailor detection to individual gas species, and extend the methodology to additional hydrocarbons. These advancements will broaden the applicability of BF-QEPAS toward comprehensive, real-time natural gas analysis in both environmental and industrial contexts.

CRediT authorship contribution statement

Luigi Melchiorre: Writing – original draft, Visualization, Methodology, Investigation, Formal analysis, Data curation. **Giansergio Menduni:** Writing – review & editing, Supervision, Methodology, Conceptualization. **Giovanni Magno:** Writing – review & editing, Validation, Resources. **Liam O'Faolain:** Writing – review & editing, Resources. **Pietro Patimisco:** Writing – review & editing, Supervision, Methodology, Funding acquisition, Conceptualization. **Vincenzo Spagnolo:** Writing – review & editing, Supervision, Project administration, Funding acquisition, Conceptualization. **Angelo Sampaolo:** Writing – review & editing, Supervision, Project administration, Methodology, Funding acquisition, Conceptualization.

Declaration of competing interest

The authors declare that they have no known competing financial interests or personal relationships that could have appeared to influence the work reported in this paper.

Acknowledgements

The authors from the Physics Department of the Polytechnic University and the University of Bari acknowledge support from the European Union's Horizon 2020 research and innovation program (Grant Agreement No. 101135764, EVOQUE); the PNRR MUR project (PE0000023, NQSTI); MUR—Dipartimenti di Eccellenza 2023–2027 (QuaSiModO, "Quantum Sensing and Modelling for One-Health"); Thorlabs GmbH through the PolySenSe joint research laboratory; the project PNC 0000001 (D3-4Health, "Digital Driven Diagnostics, Prognostics and Therapeutics for Sustainable Health Care," CUP: B83C22006120001); and the National Plan for Complementary Investments to the NRRP, funded by the European Union—NextGenerationEU, with the NRRP project "BRIEF—Biorobotics Research and Innovation Engineering Facilities" (CUP: J13C22000400007).

Data availability

Data will be made available on request.

References

[1] J. Hodgkinson, R.D. Pride, Methane-specific gas detectors: the effect of natural gas composition, Meas. Sci. Technol. 21 (2010) 105103, https://doi.org/10.1088/0957-0233/21/10/105103.

[2] K. Krzempek, R. Lewicki, L. Nähle, M. Fischer, J. Koeth, S. Belahsene, Y. Rouillard, L. Worschech, F.K. Tittel, Continuous wave, distributed feedback diode laser based sensor for trace-gas detection of ethane, Appl. Phys. B 106 (2012) 251–255, https://doi.org/10.1007/s00340-011-4857-9.

[3] T. Aldhafeeri, M.-K. Tran, R. Vrolyk, M. Pope, M. Fowler, A review of methane gas detection sensors: recent developments and future perspectives, Inventions 5 (2020) 28, https://doi.org/10.3390/inventions5030028.

[4] G. Li, Y. Wu, Z. Zhang, X. Zhang, K. Ma, Y. Jiao, J. Li, Y. Liu, Y. Song, H. Zhao, S. Zhai, Q. Li, WMS based dual-range real-time trace sensor for ethane detection in exhaled breath, Opt. Lasers Eng. 159 (2022) 107222, https://doi.org/10.1016/j.optlaseng.2022.107222.

[5] M. Kwaśny, A. Bombalska, Optical methods of methane detection, Sensors 23 (2023) 2834, https://doi.org/10.3390/s23052834.

[6] I. Karakurt, G. Aydin, K. Aydiner, Sources and mitigation of methane emissions by sectors: a critical review, Renew Energy 39 (2012) 40–48, https://doi.org/10.1016/j.renene.2011.09.006.

[7] R.O. Yusuf, Z.Z. Noor, A.H. Abba, M.A.A. Hassan, M.F.M. Din, Methane emission by sectors: a comprehensive review of emission sources and mitigation methods, Renew. Sustain. Energy Rev. 16 (2012) 5059–5070, https://doi.org/10.1016/j.rser.2012.04.008.

[8] I.J. Simpson, M.P. Sulbaek Andersen, S. Meinardi, L. Bruhwiler, N.J. Blake, D. Helmig, F.S. Rowland, D.R. Blake, Long-term decline of global atmospheric ethane concentrations and implications for methane, Nature 488 (2012) 490–494, https://doi.org/10.1038/nature11342.

[9] R.W. Howarth, A bridge to nowhere: methane emissions and the greenhouse gas footprint of natural gas, Energy Sci. Eng. 2 (2014) 47–60, https://doi.org/10.1002/ese3.35.

[10] J. Peischl, S.J. Eilerman, J.A. Neuman, K.C. Aikin, J. de Gouw, J.B. Gilman, S. C. Herndon, R. Nadkarni, M. Trainer, C. Warneke, T.B. Ryerson, Quantifying methane and ethane emissions to the atmosphere from central and western U.S oil and natural gas production regions, J. Geophys. Res.: Atmos. 123 (2018) 7725–7740, https://doi.org/10.1029/2018JD028622.

[11] L. Shao, et al., Simultaneous detection of atmospheric CO and CH4 based on TDLAS using a single 2.3 μm DFB laser, Spectrochim. Acta A Mol. Biomol. Spectrosc. 222 (Nov. 2019) 117118, https://doi.org/10.1016/j.saa.2019.05.023.

[12] M. Saunois, P. Bousquet, B. Poulter, A. Peregon, P. Ciais, J.G. Canadell, E. J. Dlugokencky, G. Etiope, D. Bastviken, S. Houweling, G. Janssens-Maenhout, F. N. Tubiello, S. Castaldi, R.B. Jackson, M. Alexe, V.K. Arora, D.J. Beerling, P. Bergamaschi, D.R. Blake, G. Brailsford, V. Brovkin, L. Bruhwiler, C. Crevoisier, P. Crill, K. Covey, C. Curry, C. Frankenberg, N. Gedney, L. Höglund-Isaksson, M. Ishizawa, A. Ito, F. Joos, H.-S. Kim, T. Kleinen, P. Krummel, J.-F. Lamarque, R. Langenfelds, R. Locatelli, T. Machida, S. Maksyutov, K.C. McDonald, J. Marshall, J.R. Melton, I. Morino, V. Naik, S. O'Doherty, F.-J.-W. Parmentier, P.K. Patra, C. Peng, S. Peng, G.P. Peters, I. Pison, C. Prigent, R. Prinn, M. Ramonet, W.J. Riley, M. Saito, M. Santini, R. Schroeder, I.J. Simpson, R. Spahni, P. Steele, A. Takizawa, B.F. Thornton, H. Tian, Y. Tohjima, N. Viovy, A. Voulgarakis, M. van Weele, G. R. van der Werf, R. Weiss, C. Wiedinmyer, D.J. Wilton, A. Wiltshire, D. Worthy, D. Wunch, X. Xu, Y. Yoshida, B. Zhang, Z. Zhang, Q. Zhu, The global methane budget 2000–2012, Earth Syst. Sci. Data 8 (2016) 697–751, https://doi.org/10.5194/essd-8-697-2016.

[13] M. Saunois, A.R. Stavert, B. Poulter, P. Bousquet, J.G. Canadell, R.B. Jackson, P. A. Raymond, E.J. Dlugokencky, S. Houweling, P.K. Patra, P. Ciais, V.K. Arora, D. Bastviken, P. Bergamaschi, D.R. Blake, G. Brailsford, L. Bruhwiler, K.M. Carlson, M. Carrol, S. Castaldi, N. Chandra, C. Crevoisier, P.M. Crill, K. Covey, C.L. Curry, G. Etiope, C. Frankenberg, N. Gedney, M.I. Hegglin, L. Höglund-Isaksson, G. Hugelius, M. Ishizawa, A. Ito, G. Janssens-Maenhout, K.M. Jensen, F. Joos, T. Kleinen, P.B. Krummel, R.L. Langenfelds, G.G. Laruelle, L. Liu, T. Machida, S. Maksyutov, K.C. McDonald, J. McNorton, P.A. Miller, J.R. Melton, I. Morino, J. Müller, F. Murguia-Flores, V. Naik, Y. Niwa, S. Noce, S. O'Doherty, R.J. Parker, C. Peng, S. Peng, G.P. Peters, C. Prigent, R. Prinn, M. Ramonet, P. Regnier, W. J. Riley, J.A. Rosentreter, A. Segers, I.J. Simpson, H. Shi, S.J. Smith, L.P. Steele, B. F. Thornton, H. Tian, Y. Tohjima, F.N. Tubiello, A. Tsuruta, N. Viovy, A. Voulgarakis, T.S. Weber, M. van Weele, G.R. van der Werf, R.F. Weiss, D. Worthy, D. Wunch, Y. Yin, Y. Yoshida, W. Zhang, Z. Zhang, Y. Zhao, B. Zheng, Q. Zhu, Q. Zhu, Q. Zhuang, The global methane budget 2000–2017, Earth Syst. Sci. Data 12 (2020) 1561–1623, https://doi.org/10.5194/essd-12-1561-2020.

[14] M. Saunois, A. Martinez, B. Poulter, Z. Zhang, P.A. Raymond, P. Regnier, J. G. Canadell, R.B. Jackson, P.K. Patra, P. Bousquet, P. Ciais, E.J. Dlugokencky, X. Lan, G.H. Allen, D. Bastviken, D.J. Beerling, D.A. Belikov, D.R. Blake, S. Castaldi, M. Crippa, B.R. Deemer, F. Dennison, G. Etiope, N. Gedney, L. Höglund-Isaksson, M.A. Holgerson, P.O. Hopcroft, G. Hugelius, A. Ito, A.K. Jain, R. Janardanan, M. S. Johnson, T. Kleinen, P.B. Krummel, R. Lauerwald, T. Li, X. Liu, K.C. McDonald, J.R. Melton, J. Mühle, J. Müller, F. Murguia-Flores, Y. Niwa, S. Noce, S. Pan, R. J. Parker, C. Peng, M. Ramonet, W.J. Riley, G. Rocher-Ros, J.A. Rosentreter, M. Sasakawa, A. Segers, S.J. Smith, E.H. Stanley, J. Thanwerdas, H. Tian, A. Tsuruta, F.N. Tubiello, T.S. Weber, G.R. van der Werf, D.E.J. Worthy, Y. Xi, Y. Yoshida, W. Zhang, B. Zheng, Q. Zhu, Q. Zhu, Q. Zhuang, Global methane budget 2000–2020, Earth Syst. Sci. Data 17 (2025) 1873–1958, https://doi.org/10.5194/essd-17-1873-2025.

[15] P. Englezos, N. Kalogerakis, P.D. Dholabhai, P.R. Bishnoi, Kinetics of formation of methane and ethane gas hydrates, Chem. Eng. Sci. 42 (1987) 2647–2658, https://doi.org/10.1016/0009-2509(87)87015-X.

[16] X. Shen, B. Zhang, X. Zhang, G. Xiu, Explosion characteristics of methane-ethane mixtures in air, J. Loss Prev. Process Ind. 45 (2017) 102–107, https://doi.org/10.1016/j.jlp.2016.11.012.

[17] J.R. Roscioli, S. Herndon, D.D. Nelson, T. Yacovitch, Methane, Ethane, and Propane Sensor for Real-time Leak Detection and Diagnostics, Argonne, IL (United States), 2017. DOI: 10.2172/1347976.

[18] A.R. Brandt, G.A. Heath, E.A. Kort, F. O'Sullivan, G. Pétron, S.M. Jordaan, P. Tans, J. Wilcox, A.M. Gopstein, D. Arent, S. Wofsy, N.J. Brown, R. Bradley, G.D. Stucky, D. Eardley, R. Harriss, Methane leaks from north American natural gas systems, Science 343 (2014) (1979) 733–735, https://doi.org/10.1126/science.1247045.

[19] A.R. Brandt, G.A. Heath, D. Cooley, Methane Leaks from Natural Gas Systems follow Extreme Distributions, Environ. Sci. Technol. 50 (2016) 12512–12520, https://doi.org/10.1021/acs.est.6b04303.

[20] C.N. Brodsky, M.D. Bucala, S.T. Rowland, D.R. Michanowicz, The burden of natural gas leaks on public sector emergency response in the United States, Energy Pol. 192 (2024) 114214, https://doi.org/10.1016/j.enpol.2024.114214.

[21] A.J. Benavides-Serrano, M.S. Mannan, C.D. Laird, A quantitative assessment on the placement practices of gas detectors in the process industries, J. Loss Prev. Process Ind. 35 (2015) 339–351, https://doi.org/10.1016/j.jlp.2014.09.010.

[22] B. Lamb, A. Guenther, D. Gay, H. Westberg, A national inventory of biogenic hydrocarbon emissions, Atmos. Environ. 21 (1987) (1967) 1695–1705, https://doi.org/10.1016/0004-6981(87)90108-9.

[23] D.A. Stolper, A.M. Martini, M. Clog, P.M. Douglas, S.S. Shusta, D.L. Valentine, A. L. Sessions, J.M. Eiler, Distinguishing and understanding thermogenic and biogenic sources of methane using multiply substituted isotopologues, Geochim. Cosmochim. Acta 161 (2015) 219–247, https://doi.org/10.1016/j.gca.2015.04.015.

[24] P.K. Sekhar, J. Kysar, E.L. Brosha, C.R. Kreller, Development and testing of an electrochemical methane sensor, Sens. Actuat. B Chem. 228 (2016) 162–167, https://doi.org/10.1016/j.snb.2015.12.100.

[25] M.J. Bezdek, S.-X.L. Luo, K.H. Ku, T.M. Swager, A chemiresistive methane sensor, Proceedings of the National Academy of Sciences 118 (2021). DOI: 10.1073/pnas.2022515118.

[26] A.F. Aldosary, M.A. Shar, H.R. AlQahtani, High-sensitivity detection of ethane and ethylene using gamma-irradiated ZnO chemiresistors, Meas.: Sens. 24 (2022) 100600, https://doi.org/10.1016/j.measen.2022.100600.

[27] G.E. Bingham, R.D. Kiefer, C.H. Gillespie, T.G. McRae, H.C. Goldwire, R. P. Koopman, Portable, fast-response gas sensor for measuring methane and ethane and propane in liquefied natural gas spills, Rev. Sci. Instrum. 54 (1983) 1356–1361, https://doi.org/10.1063/1.1137243.

[28] Z. Xi, K. Zheng, C. Zheng, H. Zhang, F. Song, C. Li, W. Ye, Y. Zhang, Y. Wang, F. K. Tittel, Near-infrared dual-gas sensor system for methane and ethane detection using a compact multipass cell, Front. Phys. 10 (2022), https://doi.org/10.3389/fphy.2022.843171.

[29] M. Winkowski, T. Stacewicz, Detection of ethane, methane, formaldehyde and water vapor in the 3.33 μm range, Metrol. Measur. Syst. (2021) 271–282, https://doi.org/10.24425/mms.2022.140033.

[30] A.A. Kosterev, Y.A. Bakhirkin, R.F. Curl, F.K. Tittel, Quartz-enhanced photoacoustic spectroscopy, Opt. Lett. 27 (2002) 1902, https://doi.org/10.1364/OL.27.001902.

[31] P. Patimisco, G. Scamarcio, F. Tittel, V. Spagnolo, Quartz-enhanced photoacoustic spectroscopy: a review, Sensors 14 (2014) 6165–6206, https://doi.org/10.3390/s140406165.

[32] A.F.P. Cantatore, G. Menduni, A. Zifarelli, P. Patimisco, M. Giglio, M. Gonzalez, H. R. Seren, P. Luo, V. Spagnolo, A. Sampaolo, Methane, ethane, and propane detection using a quartz-enhanced photoacoustic sensor for natural gas composition analysis, Energy Fuel 39 (2025) 638–646, https://doi.org/10.1021/acs.energyfuels.4c03726.

[33] Z. Shang, et al., Quartz-enhanced photoacoustic NH3 sensor exploiting a large-prong-spacing quartz tuning fork and an optical fiber amplifier for biomedical applications, Photoacoustics 26 (Jun. 2022) 100363, https://doi.org/10.1016/j.pacs.2022.100363.

[34] A.A. Kosterev, F.K. Tittel, D.V. Serebryakov, A.L. Malinovsky, I.V. Morozov, Applications of quartz tuning forks in spectroscopic gas sensing, Rev. Sci. Instrum. 76 (2005), https://doi.org/10.1063/1.1884196.

[35] Y. Ma, Review of recent advances in QEPAS-based trace gas sensing, Appl. Sci. 8 (2018) 1822, https://doi.org/10.3390/app8101822.

[36] A. Sampaolo, P. Patimisco, M. Giglio, A. Zifarelli, H. Wu, L. Dong, V. Spagnolo, Quartz-enhanced photoacoustic spectroscopy for multi-gas detection: a review, Anal. Chim. Acta 1202 (2022) 338894, https://doi.org/10.1016/j.aca.2021.338894.

[37] J. Sun, H. Deng, N. Liu, H. Wang, B. Yu, J. Li, Mid-infrared gas absorption sensor based on a broadband external cavity quantum cascade laser, Rev. Sci. Instrum. 87 (12) (2016) Dec, https://doi.org/10.1063/1.4968041.

[38] J. Li, N. Liu, J. Ding, S. Zhou, T. He, L. Zhang, Piezoelectric effect-based detector for spectroscopic application, Opt. Lasers Eng. 115 (Apr. 2019) 141–148, https://doi.org/10.1016/j.optlaseng.2018.11.020.

[39] T. Wei, et al., "High and flat spectral responsivity of quartz tuning fork used as infrared photodetector in tunable diode laser spectroscopy, Appl. Phys. Rev. 8 (4) (2021) Dec, https://doi.org/10.1063/5.0062415.

[40] Y. Pan, J. Zhao, P. Lu, C. Sima, D. Liu, Recent advances in light-induced thermoelastic spectroscopy for gas sensing: a review, Remote Sens. (Basel) 15 (1) (Dec. 2022) 69, https://doi.org/10.3390/rs15010069.

[41] L. Xu, S. Zhou, N. Liu, M. Zhang, J. Liang, J. Li, Multigas sensing technique based on quartz crystal tuning fork-enhanced laser spectroscopy, Anal. Chem. 92 (20) (Oct. 2020) 14153–14163, https://doi.org/10.1021/acs.analchem.0c03233.
[42] Q. Zhang, J. Chang, Z. Cong, J. Sun, Z. Wang, QEPAS sensor for Simultaneous measurements of H_2O, CH_4, and C_2H_2 using different QTF, IEEE Photonics J. 10 (2018) 1–8, https://doi.org/10.1109/JPHOT.2018.2880187.
[43] M. Olivieri, A. Zifarelli, G. Menduni, M. Di Gioia, C. Marzocca, V.M.N. Passaro, A. Sampaolo, M. Giglio, V. Spagnolo, P. Patimisco, Influence of air pressure on the resonance properties of a T-shaped quartz tuning fork coupled with resonator tubes, Appl. Sci. 11 (2021) 7974, https://doi.org/10.3390/app11177974.
[44] R. Rousseau, N. Maurin, W. Trzpil, M. Bahriz, A. Vicet, Quartz tuning fork resonance tracking and application in quartz enhanced photoacoustics spectroscopy, Sensors 19 (2019) 5565, https://doi.org/10.3390/s19245565.
[45] H. Wu, L. Dong, H. Zheng, Y. Yu, W. Ma, L. Zhang, W. Yin, L. Xiao, S. Jia, F. K. Tittel, Beat frequency quartz-enhanced photoacoustic spectroscopy for fast and calibration-free continuous trace-gas monitoring, Nat. Commun. 8 (2017) 15331, https://doi.org/10.1038/ncomms15331.
[46] B. Li, G. Menduni, M. Giglio, P. Patimisco, A. Sampaolo, A. Zifarelli, H. Wu, T. Wei, V. Spagnolo, L. Dong, Quartz-enhanced photoacoustic spectroscopy (QEPAS) and beat frequency-QEPAS techniques for air pollutants detection: a comparison in terms of sensitivity and acquisition time, Photoacoustics 31 (2023) 100479, https://doi.org/10.1016/j.pacs.2023.100479.
[47] H. Wu, L. Dong, X. Yin, H. Zheng, S. Jia, F.K. Tittel, Fast and calibration-free trace-gas monitoring based on beat frequency quartz-enhanced photoacoustic spectroscopy, in: Imaging and Applied Optics 2018 (3D, AO, AIO, COSI, DH, IS, LACSEA, LS&C, MATH, PcAOP), OSA, Washington, D.C., 2018: p. SM3H.5. DOI: 10.1364/LSC.2018.SM3H.5.
[48] W. Ye, W. Liu, W. Luo, J. Xiao, L. He, Y. Huang, D. Zhu, Calibration-free near-infrared methane sensor system based on BF-QEPAS, Infrared Phys. Technol. 133 (2023) 104784, https://doi.org/10.1016/j.infrared.2023.104784.
[49] J. Du, S. Xia, K. Cheng, M. Zhang, J. Li, Quartz crystal tuning fork enhanced spectroscopy with self-calibration algorithms, Sens. Actuat. B Chem. 430 (May 2025) 137344, https://doi.org/10.1016/j.snb.2025.137344.
[50] G. Menduni, F. Sgobba, S. Dello Russo, A.C. Ranieri, A. Sampaolo, P. Patimisco, M. Giglio, V.M.N. Passaro, S. Csutak, D. Assante, E. Ranieri, E. Geoffrion, V. Spagnolo, Fiber-coupled quartz-enhanced photoacoustic spectroscopy system for methane and ethane monitoring in the near-infrared spectral range, Molecules 25 (2020) 5607, https://doi.org/10.3390/molecules25235607.
[51] I.E. Gordon, L.S. Rothman, R.J. Hargreaves, R. Hashemi, E.V. Karlovets, F.M. Skinner, E.K. Conway, C. Hill, R.V. Kochanov, Y. Tan, P. Wcisło, A.A. Finenko, K. Nelson, P.F. Bernath, M. Birk, V. Boudon, A. Campargue, K.V. Chance, A. Coustenis, B.J. Drouin, J. –M. Flaud, R.R. Gamache, J.T. Hodges, D. Jacquemart, E. J. Mlawer, A.V. Nikitin, V.I. Perevalov, M. Rotger, J. Tennyson, G.C. Toon, H. Tran, V.G. Tyuterev, E.M. Adkins, A. Baker, A. Barbe, E. Canè, A.G. Császár, A. Dudaryonok, O. Egorov, A.J. Fleisher, H. Fleurbaey, A. Foltynowicz, T. Furtenbacher, J.J. Harrison, J. –M. Hartmann, V. –M. Horneman, X. Huang, T. Karman, J. Karns, S. Kassi, I. Kleiner, V. Kofman, F. Kwabia–Tchana, N.N. Lavrentieva, T.J. Lee, D.A. Long, A.A. Lukashevskaya, O.M. Lyulin, V.Yu. Makhnev, W. Matt, S.T. Massie, M. Melosso, S.N. Mikhailenko, D. Mondelain, H.S.P. Müller, O.V. Naumenko, A. Perrin, O.L. Polyansky, E. Raddaoui, P.L. Raston, Z.D. Reed, M. Rey, C. Richard, R. Tóbiás, I. Sadiek, D.W. Schwenke, E. Starikova, K. Sung, F. Tamassia, S.A. Tashkun, J. Vander Auwera, I.A. Vasilenko, A.A. Vigasin, G.L. Villanueva, B. Vispoel, G. Wagner, A. Yachmenev, S.N. Yurchenko, The HITRAN2020 molecular spectroscopic database, J Quant Spectrosc Radiat Transf 277 (2022) 107949. DOI: 10.1016/j.jqsrt.2021.107949.
[52] L.G. Smith, The Infra-Red Spectrum of C2H6, J. Chem. Phys. 17 (1949) 139–167, https://doi.org/10.1063/1.1747206.
[53] M. Hepp, M. Herman, Vibration-rotation bands in ethane, Mol. Phys. 98 (2000) 57–61, https://doi.org/10.1080/00268970009483269.
[54] X. Tian, Y. Cao, J. Chen, K. Liu, G. Wang, T. Tan, J. Mei, W. Chen, X. Gao, Dual-gas sensor of CH4/C2H6 based on wavelength modulation spectroscopy coupled to a home-made compact dense-pattern multipass cell, Sensors 19 (2019) 820, https://doi.org/10.3390/s19040820.
[55] Acoustic Detection Module for QEPAS, (n.d.). https://www.thorlabs.com/newgrouppage9.cfm?objectgroup_id=11241&pn=ADM01 (accessed June 12, 2025).
[56] A.L. Chakraborty, A. Roy, Wavelength Modulation Spectroscopy, in: 2021: pp. 321–362. DOI: 10.1007/978-981-33-6084-6_13.
[57] P. Kluczynski, J. Gustafsson, Å.M. Lindberg, O. Axner, Wavelength modulation absorption spectrometry — an extensive scrutiny of the generation of signals, Spectrochim Acta Part B At Spectrosc 56 (2001) 1277–1354, https://doi.org/10.1016/S0584-8547(01)00248-8.
[58] K. Song, E.C. Jung, Recent developments in modulation spectroscopy for trace gas detection using tunable diode lasers, Appl. Spectrosc. Rev. 38 (2003) 395–432, https://doi.org/10.1081/ASR-120026329.
[59] F. Sgobba, G. Menduni, S. Dello Russo, A. Sampaolo, P. Patimisco, M. Giglio, E. Ranieri, V.M.N. Passaro, F.K. Tittel, V. Spagnolo, Quartz-enhanced photoacoustic detection of ethane in the near-IR exploiting a highly performant spectrophone, Appl. Sci. 10 (2020) 2447, https://doi.org/10.3390/app10072447.
[60] P. Luo, J. Harrist, G. Menduni, R. Mesdour, N. StMichel, A. Sampaolo, Simultaneous detection of methane, ethane, and propane by QEPAS sensors for on-site hydrocarbon characterization and production monitoring, ACS Omega 7 (2022) 3395–3406, https://doi.org/10.1021/acsomega.1c05645.
[61] A. Zifarelli, G. Negro, L.A. Mongelli, A. Sampaolo, E. Ranieri, L. Dong, H. Wu, P. Patimisco, G. Gonnella, V. Spagnolo, Effect of gas turbulence in quartz-enhanced photoacoustic spectroscopy: a comprehensive flow field analysis, Photoacoustics 38 (2024) 100625, https://doi.org/10.1016/j.pacs.2024.100625.
[62] A. Zifarelli, A. Sampaolo, P. Patimisco, M. Giglio, M. Gonzalez, H. Wu, L. Dong, V. Spagnolo, Methane and ethane detection from natural gas level down to trace concentrations using a compact mid-IR LITES sensor based on univariate calibration, Photoacoustics 29 (2023) 100448, https://doi.org/10.1016/j.pacs.2023.100448.

Glossary

1f: First harmonic.
2f: Second harmonic.
ADM: Acoustic detection module.
BF: Beat-frequency.
C: Carbon.
C1: Methane.
C2: Ethane.
C_2H_6: Ethane.
CH_4: Methane.
DFB: Distributed-feedback.
f_r: Resonance frequency.
H: Hydrogen.
IR: Infrared.
MDL: Minimum detection limit.
N_2: Nitrogen
pp: Peak-to-peak.
ppm: Parts-per-million.
Q: Quality factor.
QEPAS: Quartz-enhanced photoacoustic spectroscopy.
QTF: Quartz tuning fork.
R^2: Coefficient of determination.
SCCM: Standard cubic centimeters per minute.
SNR: Signal-to-noise ratio.
WMS: Wavelength modulation spectroscopy.

Luigi Melchiorre was born in Acquaviva delle Fonti, Bari, Italy, on September 28, 1996. He received the B.Sc. in Electronic and Telecommunications Engineering from the Polytechnic University of Bari, Italy, in 2019, and the M.Sc. in Telecommunications Engineering from the same institution in 2022. He is currently pursuing the Ph.D. in Industry 4.0 at the Polytechnic University of Bari. Since November 2022, he has been working with the PolySenSe Laboratory at the Physics Department and the nPEG Group at the Electrical and Information Engineering Department at the Polytechnic University of Bari. His research activities focus on developing innovative optical gas sensors that exploit quartz-enhanced photoacoustic spectroscopy (QEPAS) and light-induced thermoelastic spectroscopy (LITES) techniques. His work involves designing, characterizing, and implementing trace gas optical sensors through photonic integration and non-linear optics approaches. His current research interests feature gas sensing technologies for industrial, environmental, chemical, and medical applications.

Giansergio Menduni received the M.Sc. (*cum laude*) in 2017 and the Ph.D. in 2021 in Electronic Engineering from the Polytechnic University of Bari, Italy. Since 2022, he has been an Assistant Professor in Applied Physics at the Physics Department of Polytechnic University of Bari. His research activity is focused on the development of gas sensors based on quartz-enhanced photoacoustic spectroscopy (QEPAS) and light-induced thermoelastic spectroscopy (LITES) on the signal conditioning of quartz tuning forks transducers.

Giovanni Magno is an Assistant Professor in Electromagnetic Fields at the Polytechnic University of Bari, Italy. He received the M.Sc. in Electronic Engineering (2011) and the Ph.D. in Electrical and Information Engineering (2015) from Polytechnic University of Bari. From 2015 to 2020, he was a researcher at C2N–CNRS, France. His research focuses on the design and characterization of optical and microwave devices, including plasmonic structures, photonic crystals, optical and microwave metasurfaces, antennas and nanoantennas, reconfigurable graphene-based devices, electromagnetic sensing, and nanotweezers. He has co-authored over 100 publications and serves as Academic Editor for the International Journal of Optics and the International Journal of Antennas and Propagation (Wiley).

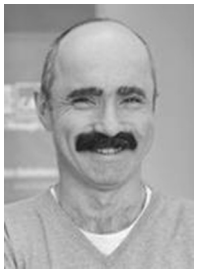

Liam O'Faolain received his Ph.D. degree in Physics from the University of St Andrews in 2005 and he leads the Nanophotonics Group at the Centre for Advanced Photonics and Process Analysis (CAPPA) in Munster Technological University (MTU). His research focuses on nanophotonics and integrated photonics, with applications in efficient laser design and photonic sensing. He spent 15 years at the University of St Andrews. He joined the group of Prof. David A. B. Miller at Stanford University in 2012 as an SU2P Entrepreneurial Fellow before returning to St Andrews as a lecturer in 2013. He relocated his research group to MTU in 2016 (www.cappa.ie). He has published over 140 peer-reviewed journal papers.

Pietro Patimisco obtained the M.Sc. (*cum laude*) in Physics in 2009 and the Ph.D. in Physics in 2013 from the University of Bari. Since 2023, he is an Associate Professor at the Physics Department of the University of Bari. He was a visiting scientist in the Laser Science Group at Rice University in 2013 and 2014. The main scientific skills of Pietro Patimisco are related to the development of spectroscopic techniques for studying the light–matter interaction in the infrared range. Prof. Pietro Patimisco is co-founder of "PolySenSe Innovations", an academic spin-off devoted to the development of optical-based sensors.

Vincenzo Spagnolo received the degree (*summa cum laude*) and the Ph.D., both in Physics, from the University of Bari. He works as Full Professor of Applied Physics at the Polytechnic University of Bari. In 2019, he become Vice-Rector of the Polytechnic University of Bari, deputy to Technology Transfer. Since 2017, he is the director of the joint-research lab PolySenSe, created by Thorlabs GmbH and Polytechnic University of Bari, devoted to the development and implementation of novel gas sensing techniques and the realization of highly sensitive quartz-enhanced photoacoustic spectroscopy (QEPAS) trace-gas sensors.

Angelo Sampaolo obtained his M.S. degree in Physics in 2013 and the Ph.D. degree in Physics in 2017 from the University of Bari. He was an associate researcher in the Laser Science Group at the Rice University from 2014 to 2016 and associate researcher at the Shanxi University since 2018. Since 2019, he has been Assistant Professor at the Polytechnic University of Bari. His research activity has focused on the development of innovative techniques in trace gas sensing, based on quartz-enhanced photoacoustic spectroscopy (QEPAS) and covering the full spectral range from near-IR to THz.